Proceedings of IMECE2009
2009 ASME International Mechanical Engineering Congress and Exposition
November 13-19, Lake Buena Vista, Florida, USA

IMECE2009-12773

SIMULATION OF COMBUSTION AND THERMAL-FLOW INSIDE A PYROSCRUBBER

Zhao Lei and Ting Wang
Energy Conversion and Conservation Center
University of New Orleans
New Orleans, LA 70148-2220, USA

ABSTRACT

A pyroscrubber is the device used in petroleum coke Calcining industry to oxidize the carbonaceous contents, including hydrocarbon volatiles of the exhaust gas from the calcination kiln, so as to recover energy to produce electricity and leave no more than small traces of unburned volatiles, solid carbon, ashes, or emissions (e.g. CO, NO_x and SO_x) in the flue gas finally discharged.

Motivated by the need to maximize the energy recovery and reduce pollutant emission from the pyroscrubber, a 3-D computational model is developed to simulate the combustion and thermal-flow phenomena inside the pyroscrubber to help seek means to reduce emissions and increase energy density for downstream power generation.

CFD model validation is achieved by comparing baseline case results with the plant measurement data of temperature and NO_x emission. The simulation results show that the specially designed high-bay wall structure generates a strong mixing zone forcing combustion to happen at an earlier stage and helps to efficiently utilize the main chamber space. A well balanced amount of excess air is favorable in generating more energy output and lowering NO_x emission. Incomplete combustion with sub-stoichiometric air cuts NO_x emission, but leads to less total energy output, lowers gas temperature and increased CO emission. A multistage burning strategy is introduced and studied and results show it successfully cuts emission without compromising energy (electricity power) output.

INTRODUCTION

A pyroscrubber is namely a furnace burning carbon particles in a stream of waste gas, particularly from a petroleum coke calcination kiln or hearth. The schematic of the calcining process for petroleum coke is shown in Fig. 1. The combusted hot gases from the pyroscrubber are ducted through a boiler to produce steam that is used to generate electricity through steam turbines. A pyroscrubber typically comprises of a U-shaped combustion chamber having a first passage arranged parallel with (preferably above) a second passage, so there is a reversal in gas flow direction between the two passages. The main function of the pyroscrubber is to oxidize the carbonaceous contents, including hydrocarbon volatiles in the exhaust gas from the calcination kiln, so as to recover energy from the waste stream and leave no more than small traces of unburned volatiles, solid carbon, ashes, or emissions (e.g. CO, NO_x and SO_x) in the flue gas finally discharged [3].

Pyroscrubbers of different designs have been employed worldwide to compete for more efficient and cleaner combustion of exhaust gases from coke calcination kilns or hearths. But very limited literature can be found about pyroscrubber design and studies from public resources.

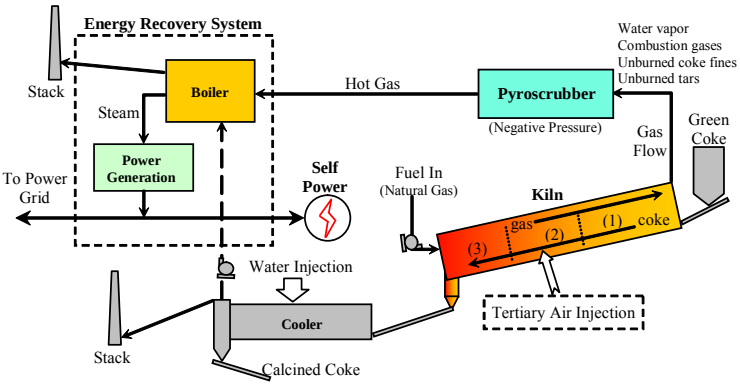

Fig. 1 Schematic of the calcining process for petcoke

To maximize the energy recovery and reduce pollutant emission from the pyroscrubber, more detailed information and a better understanding of thermal-flow and combustion process inside the pyroscrubber are needed. The objective of this study is to employ computational fluid dynamics (CFD) technique with the appropriate combustion model to better understand the combustion and thermal-flow phenomena

inside the pyroscrubber, and investigate further the potential means to improve combustion performance and reduce emissions. The specific goals are:

1. Develop a numerical model of the pyroscrubber that adequately simulates the thermal-flow and combustion processes.
2. Investigate flow pattern, temperature distribution, combustion process, and emission information inside the pyroscrubber.
3. Study the effect of different amounts of air injection with respect to combustion efficiency, energy output and NO_x emission.
4. Simulate and study the effect of introducing a multistage burning strategy on emission control and energy output.

MODELING AND METHODOLOGY

The pyroscrubber investigated in this study is shown in Figs. 2 and 3. Geometric information of the pyroscrubber is obtained through the blueprints of a calcination plant in Louisiana. The modeled domain includes part of the calcining kiln, settling chamber, inlet duct (which connects the settling chamber with the main chamber), air injection section, main chamber, and outlet duct, connecting the main chamber to the boiler. The main chamber is around 35 ft wide, 103 ft long and 40 ft tall. Details of the air injectors and the burner are shown in Fig. 3.

The inlet of the pyroscrubber receives exhaust gases from the exit of the calcining kiln. After completion of the calcining process inside the kiln, combustion product gases, together with unburned volatiles and coke fines are fed into the pyroscrubber through the settling chamber and the inlet duct. Air is injected into the main chamber through two air injection sections. The first air injection section consists of 28 air injection tubes shooting at 45^o from the vertical direction (Y direction). Not only is the second air-injection section, located at the burner slots on the east wall of the main chamber, used to inject natural gas as the start-up fuel, but they also blow air into the main chamber after the ignition and start-up process complete. Hot product gases exit the pyroscrubber main chamber through the outlet duct and are fed into the steam boiler to generate electricity.

The major characteristics and general assumptions in this study are listed below:

1. The flow inside the pyroscrubber is three dimensional, incompressible, and turbulent.
2. Gas species involved in this study are Newtonian fluids with variable properties as functions of temperature.
3. Buoyancy and radiation effects are considered.
4. Non-slip and adiabatic wall conditions are assumed.

The CFD commercial software FLUENT (version 6.2.16) is used. The simulation uses the segregated solver, which employs an implicit pressure-correction scheme. The SIMPLE algorithm is used to couple the pressure and velocity. Second order upwind scheme is selected for spatial discretization of the convective terms and species. Converged results are obtained after the specified residuals are met. A converged result renders mass residual of 10^{-4}, energy residual of 10^{-6}, and momentum and turbulence kinetic energy residuals of 10^{-5}. These residuals are the summation of the imbalance for each cell, scaled by a representative of the flow rate. Typically, 8,000 to 12,000 iterations are needed to obtain a converged result, which takes about 15~20 hours on a 10-node computer cluster of parallel computation with each node a 2.8 GHz Pentium personal computer.

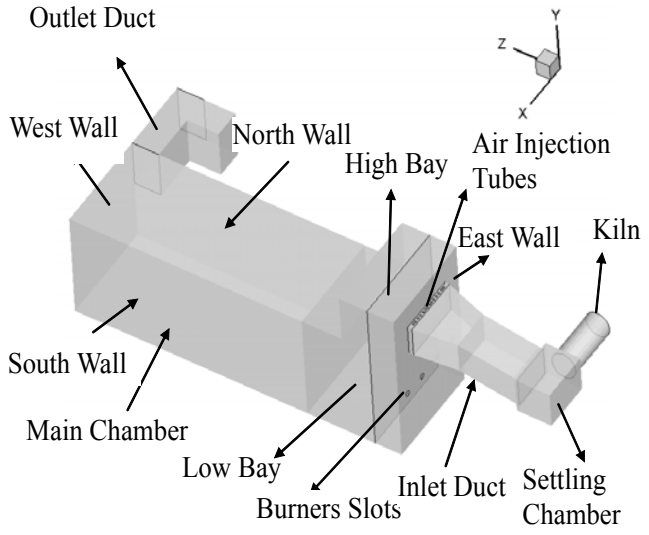

Fig. 2 A 3-D view of the pyroscrubber

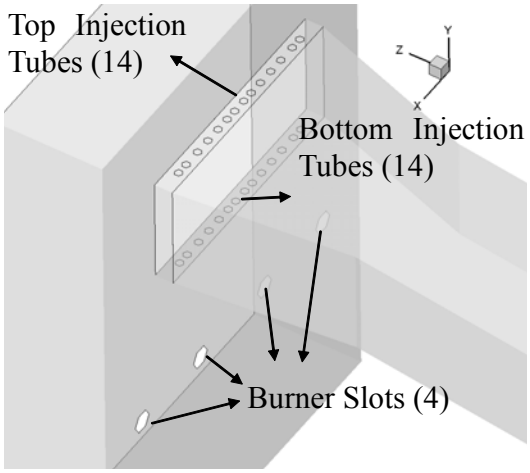

Fig. 3 Detailed air injections and burners

Governing Equations

The general conservation equations for mass, momentum and energy in general forms are shown below.

$$\frac{\partial \rho}{\partial t} + \nabla \bullet (\rho \bar{v}) = 0 \qquad (1)$$

$$\frac{\partial}{\partial t}(\rho\vec{v}) + \nabla \bullet (\rho\vec{v}\vec{v}) = -\nabla p + \nabla \bullet \left(\bar{\bar{\tau}}\right) + \rho\vec{g} + \vec{F} \quad (2)$$

$$\frac{\partial}{\partial t}(\rho E) + \nabla \bullet \left(\vec{V}(\rho E + p)\right) = \nabla \bullet \left(k_{eff}\nabla T - \sum_j h_j \vec{J}_j + \left(\bar{\bar{\tau}}_{eff} \bullet \vec{v}\right)\right) + S_h \quad (3)$$

In this study, the steady-state solution for the conservation equations is solved, so the transient terms in the equations are not included in the computation. The momentum equations are solved with the complete three-dimensional Navier-Stokes equations, so $\bar{\bar{\tau}}$, the stress tensor is given by

$$\bar{\bar{\tau}} = \mu\left[\left(\nabla\vec{v} + \nabla\vec{v}^T\right) - \frac{2}{3}\nabla \bullet \vec{v} \bullet I\right] \quad (4)$$

where I is the unit tensor.

In the energy equation, E is given as

$$E = h - \frac{p}{\rho} + \frac{v^2}{2} \quad (5)$$

"h" is the sensible enthalpy and for incompressible flow and it is given as

$$h = \sum_j Y_j h_j + \frac{p}{\rho} \quad (6)$$

$$h_j = \int_{T_{ref}}^{T} c_{p,j} dT \quad (7)$$

T_{ref} is the reference temperature, taken as 298.15 K. S_h in the energy equation is the source term and is provided by the net enthalpy formation rates from the species transport reactions.

Inlet Condition

The composition of the pyroscrubber inlet species is complex due to the calcining and combustion process inside the kiln. Since their quantities are not available from any known sources, the inlet condition is prone to uncertainty. Therefore, a sound estimate of the inlet species is critical for conducting an appropriate simulation. The inlet condition of the pyroscrubber is based on information from three sources: (a) the electric power output from the steam power plant, (b) the computational simulation results of the rotary kiln from a previous report by Zhang and Wang [10], and (c) the model from report [4]. Based on the three sources, the following assumptions are made in this study:

1. The green coke feed rate is 9.3 kg/s, of which 6% is moisture. After the moisture is driven off, 8% (7.52 % of total green coke mass) is volatiles. So the total volatiles feed rate of the kiln is 9.3 kg/s x 0.94 x 0.08 = 0.6994 kg/s, of which 40% (0.28 kg/s) is burned in the kiln and 60% (0.42 kg/s) goes into the pyroscrubber.

2. Coke fines are entrained into the pyroscrubber at the rate of 1.54kg/s.

3. All the other gas species feeding rates into the pyroscrubber follow the results given by Zhang and Wang [10] as listed in Table 1.

The species composition and feeding rate at the main inlet, air injection tubes and burner slots are summarized in Table 2. Other boundary conditions of different surfaces are listed below:

1. Inlet temperature:
   a. Main inlet gases: 500 K (440.33 °F).
   b. Air from the injection tubes: 300 K (80.33 °F)
   c. Air from the burner slots: 300 K (80.33 °F)

2. Pressure outlet -- The outlet is defined with the constant pressure. The pressure, temperature, and species mass fraction of the mixture of the potential reverse flow (if it occurs) are specified as follows:
   a. Gas outlet: Constant pressure outlet condition, P=1atm
   b. Reversed flow temperature condition, T_{outlet} = 1000K (1340.33 °F)
   c. Reversed flow mass fraction:O_2 = 0.23 and N_2= 0.77

3. Wall -- The walls are treated as adiabatic with no-slip velocity condition:
   a. Adiabatic wall condition, heat flux = 0
   b. No slip condition at the walls, u = 0, v = 0, w = 0

Table 1 Kiln exit species composition summary from [10]

species	mass fraction	mass flow rate(kg/s)	standard state enthalpy (J/kgmol)	energy released through complete combustion (J/kg-fuel)	total energy released(MW)
N_2	0.709	9.091	0	-	-
CH_4	0.000	0.000	-7.49E+07	-	-
C	0.001	0.017	-101.268	3.28E+07	0.554
H_20	0.075	0.964	-2.42E+08	-	-
CO_2	0.197	2.520	-3.94E+08	-	-
O_2	0.010	0.127	0	-	-
volatiles	0.008	0.099	-5.60E+07	4.12E+07	4.100
total	1.000	12.818	-	-	4.654

Table 2 Inlet species composition summary for 3 cases

inlet species	mass flow(kg/s)	mass fraction	stoichiometric air needed (kg/s)	80% air (kg/s)	150% air (kg/s)
N_2	9.070	0.622	0.000	same as inlet condition in stoichiometric case	
CH_4	0.000	0.000	0.000		
C	1.537	0.105	17.669		
H_20	1.154	0.079	0.000		
CO_2	2.159	0.148	0.000		
O_2	0.237	0.016	(1.021)		
volatiles	0.419	0.029	5.719		
total	14.577	1.000	22.366		
burner air	11.483	0.513	11.483	9.186	17.224
top air inject	5.442	0.243	5.442	4.353	8.163
bottom air inject	5.442	0.243	5.442	4.353	8.163

Combustion Model

In this study, gas combustion model is employed by introducing the concept of "instantaneous gasification." Carbon fines are made to gasify instantaneously, thus the combustion process can be modeled as homogeneous combustion reactions. This approach is based on the locally-homogeneous flow (LHF) model proposed by Faeth [11], implying infinitely-fast interphase transport rates. The instantaneous gasification model can effectively reveal the overall combustion process and results without dealing with the details of the otherwise complicated heterogeneous particle surface reactions, heat transfer, species transport and particle tracking in turbulent reacting flow. Featured with simpler mechanism, the gas combustion model is robust and less costly in computation. But it should be noted that this model lacks accuracy and details in describing the physical process when *reaction mechanism* is one's study interest, in which case a complete simulation of homogeneous and heterogeneous particle reactions in turbulent flow is necessary and can be found in Zhao and Wang [9].

In this study, the combustion of volatiles and gasified carbon is modeled by a single-step reaction. The mixing and transport of chemical species is modeled by solving the conservation equations describing convection, diffusion, and reaction sources for each component species. The species transport equations are solved by predicting the local mass fraction of each species, Y_i, through the solution of a convection-diffusion equation for the i-th species. The species transport equation in general form is given as:

$$\frac{\partial}{\partial t}(\rho Y_i) + \nabla \bullet (\rho \vec{v} Y_i) = -\nabla \bullet \vec{J}_i + R_i + S_i \qquad (8)$$

where R_i is the net rate of production of species i by chemical reaction. S_i is the rate of creation (a source term) from the dispersed phase. $\vec{J}_i$ is the diffusion flux of species i, which arises due to concentration gradients. For turbulent flows, mass diffusion flux is given as

$$\vec{J}_i = -\left(\rho D_{i,m} + \frac{\mu_t}{Sc_t} \right) \nabla Y_i \qquad (9)$$

where Sc_t is the turbulent Schmidt number given as $\mu_t / \rho D_t$, where μ_t is the turbulent viscosity and D_t is the turbulent diffusivity.

In this study, the reaction rate that appears as a source term in (8) is given by the turbulence-chemistry interaction model called the eddy-dissipation model as described in Magnussen [8]. The overall rate of reaction for the fastest burning fuels is controlled by turbulent mixing. The net rate of production of species i due to reaction r, $R_{i,r}$, is given by the smaller of the two given expressions below:

$$R_{i,r} = \nu'_{i,r} M_{w,i} A \rho \frac{\varepsilon}{\kappa} \min_R \left(\frac{Y_R}{\nu'_{R,r} M_{w,R}} \right) \qquad (10)$$

$$R_{i,r} = \nu'_{i,r} M_{w,i} A B \rho \frac{\varepsilon}{\kappa} \frac{\sum_P Y_P}{\sum_j^N \nu''_{j,r} M_{w,j}} \qquad (11)$$

where

Y_P is the mass fraction of any product species, P

Y_R is the mass fraction of a particular reactant, R

A is an empirical constant equal to 4.0

B is an empirical constant equal to 0.5

$\nu'_{i,r}$ is the stoichiometric coefficient for reactant i in reaction r

$\nu''_{j,r}$ is the stoichiometric coefficient for product j in reaction r

In the above equations (10) and (11), the chemical reaction rate is governed by the large-eddy mixing time scale, κ/ε, and an ignition source is not required. This is based on the assumption that the chemical reaction is much faster than the turbulence mixing time scale, so the actual chemical reaction is not important.

The complete stoichiometric global combustion equations are given below:

$$CH_{3.086}O_{0.131} + 1.706O_2 \rightarrow CO_2 + 1.543H_2O \qquad (12)$$

$$C + O_2 \rightarrow CO_2 \qquad (13)$$

NO_x Model

NOx emission consists of mostly nitric oxide (NO). Less significant are nitrogen oxide, NO_2 and nitrous oxide (N_2O). To predict NO_x emission, transport equations for NO_x concentration are solved. Since NO_x concentrations generated in a combustion system are generally low, NO_x chemistry has negligible influence on the predicted flow fields and species concentrations. Therefore, in this study the calculation of NO_x concentrations are post-processed after the thermal flow and major species concentrations are computed. The mass transport equation for the NO_x species is solved taking into account of convection, diffusion, production and consumptions of NO_x and related species. Two major NO_x generation mechanisms are modeled in this study: thermal NO_x and prompt NO_x. Details of the NO_x generation models can be found in [6]. More supporting references for the models can be found from [1], [2], [5] and [7].

Grid and Meshes

The grid used in this study is generated using GAMBIT (version 2.2.30). Structured grids are employed in meshing the kiln, part of the main chamber, and the outlet duct. Unstructured grids are employed for all the other parts, namely the settling chamber, inlet duct, and part of the main chamber. All together there are 70,729 nodes, 708,418 faces and 340,800 cells. Meshes of each part are shown in detail in Fig. 4.

Grid Sensitivity Study

A grid sensitivity study of two different mesh numbers (325,431 and 968,235) has been performed and investigated. The computational time for the low mesh number case is about 20 hours and for the high mesh number case is about 60 hours in a parallel-processed 10-node cluster. The temperature variation within the whole domain lies within 50K to 150K (2.6%-7.9%). At the exit, the difference of mass weighted temperature is about 90K (4.7%). Although the grid independency has not been achieved, for the purpose of

current study, 10% of computational uncertainty is acceptable. Therefore the mesh number around 340,000 is used for this study to save 66% of the computational time.

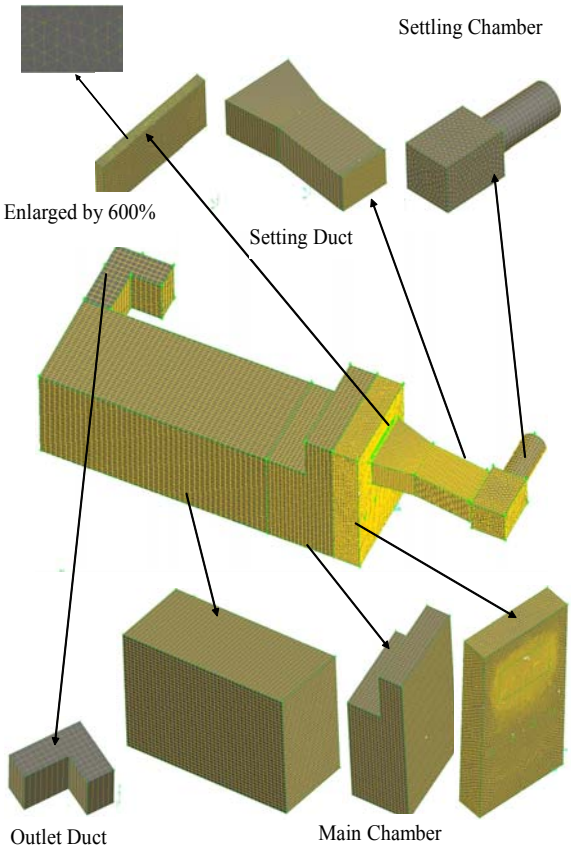

Fig.4 Meshes of different parts of the pyroscrubber

RESULTS AND DISCUSSION

In this study, a total of four cases are examined.

Case 1. Baseline case two-stage combustion (100% stoichiometric air distributed as 51% and 49%)

Case 2. 80% stoichiometric air combustion (for both stages.)

Case 3. 150% stoichiometric air combustion (for both stages.)

Case 4. Three-stage combustion (100% stoichiometric air distributed as 41%, 39% and 20%)

Case 1: Baseline Case

The 3-D results provide a clear view of flow field and temperature distribution in the pyroscrubber. Temperature contours of different planes are shown in Fig. 5. Three groups of planes are shown in the direction of X (horizontal), Y (vertical), and Z (main flow direction in the chamber) respectively. Figure 6 shows the representative pathlines. Velocity profiles of different planes in X, Y, Z directions are shown in Figs. 7, 8, and 9, respectively. Figures 10 and 11 present species concentrations and temperature distributions in X and Z directions.

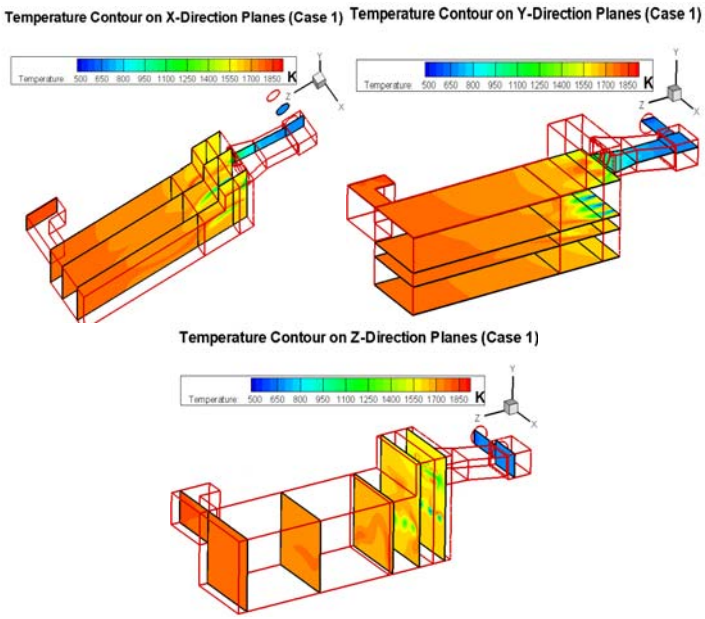

Fig. 5 Temperature contours inside the pyroscrubber at different planes for the baseline case

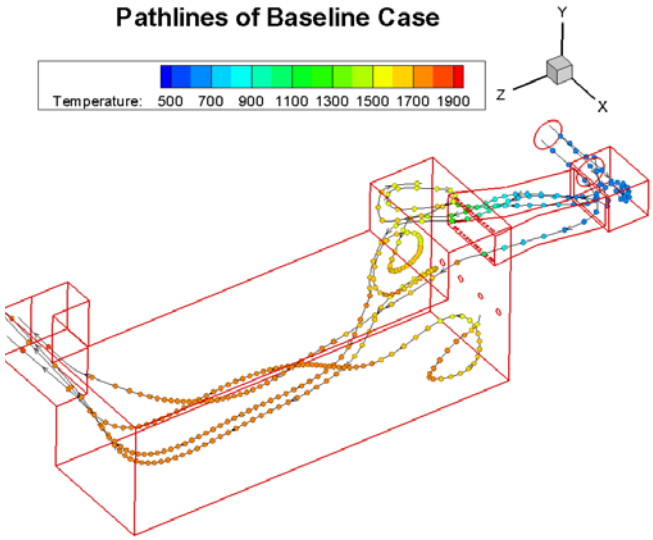

Fig. 6 Representative pathlines for the baseline case (100% stoichiometric air)

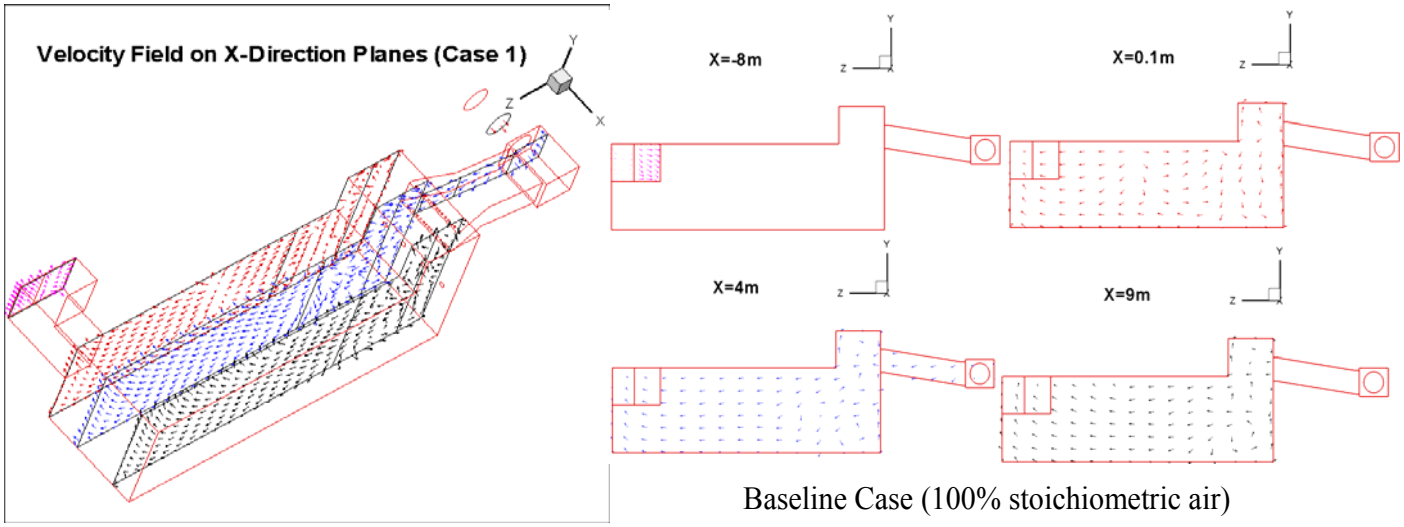

Fig. 7 Velocity field on X-direction planes for the baseline case (100% stoichiometric air)

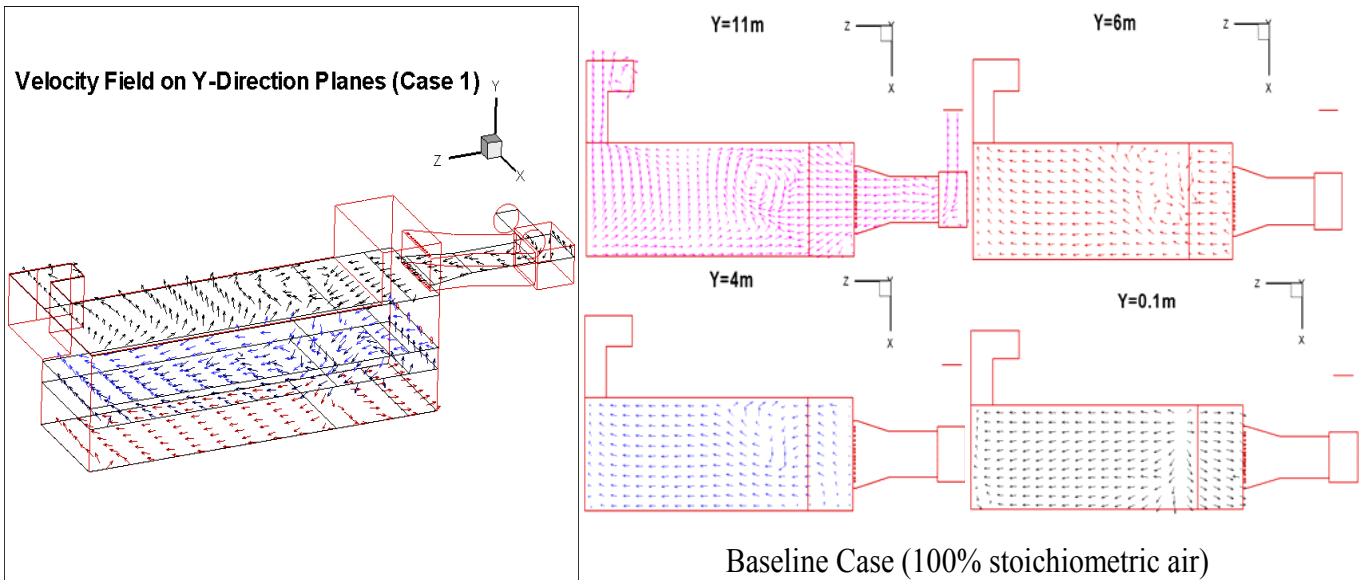

Fig. 8 Velocity field on Y-direction planes for the baseline case (100% stoichiometric air)

There are three flow streams coming into the main chamber: the first stream comes from the kiln through the inlet duct carrying all the fuels (carbon dusts and volatiles); the second stream is air injected from 28 injection tubes surrounding the high-bay duct for mixing enhancement, and the third air stream comes from the burners at the east wall of the main chamber. The burners supply natural gas fuel during start-up and only provide air during normal operation. The air injection distribution generates two different combustion situations. In the high bay area, the fuel is well mixed with a less-than-stoichiometric amount of air before the combustion starts. The combustion pattern is characterized as pre-mixed and fuel rich. Almost all the volatiles are burned in the high bay area. In the low bay area, air is injected into the chamber and interacts with the leftover fuel (mostly carbon dusts) from the top, generating the non-premixed and oxygen rich diffusion type combustion.

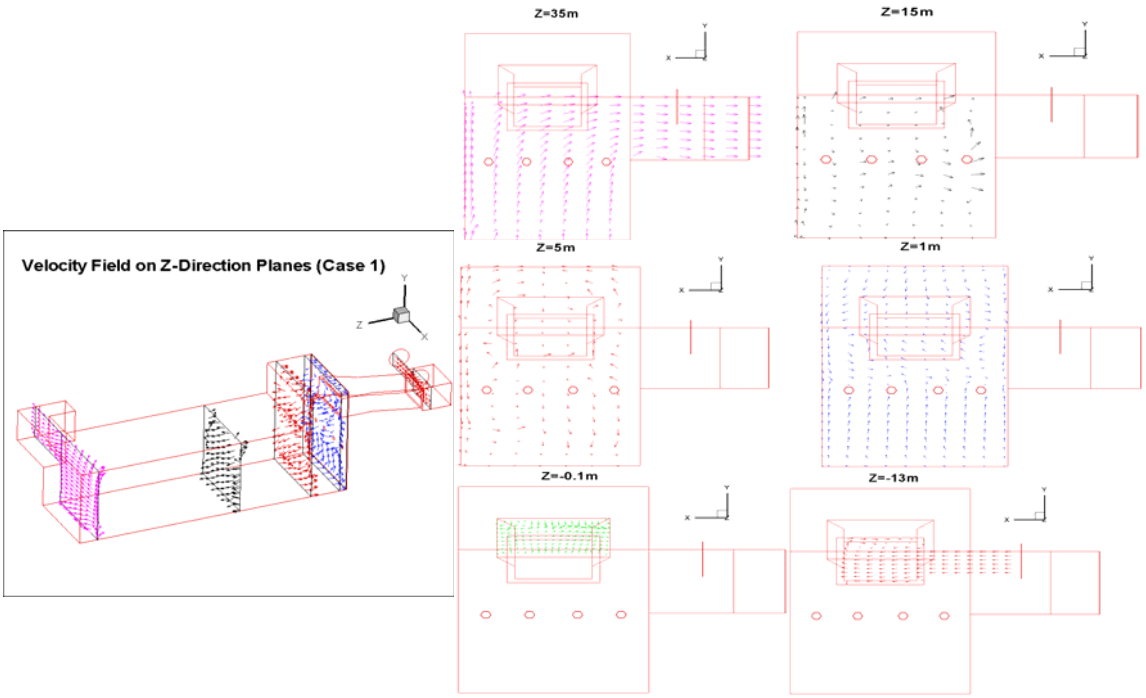

Baseline Case (100% stoichiometric air)

Fig. 9 Velocity field on Z-direction planes for the baseline case (100% stoichiometric air)

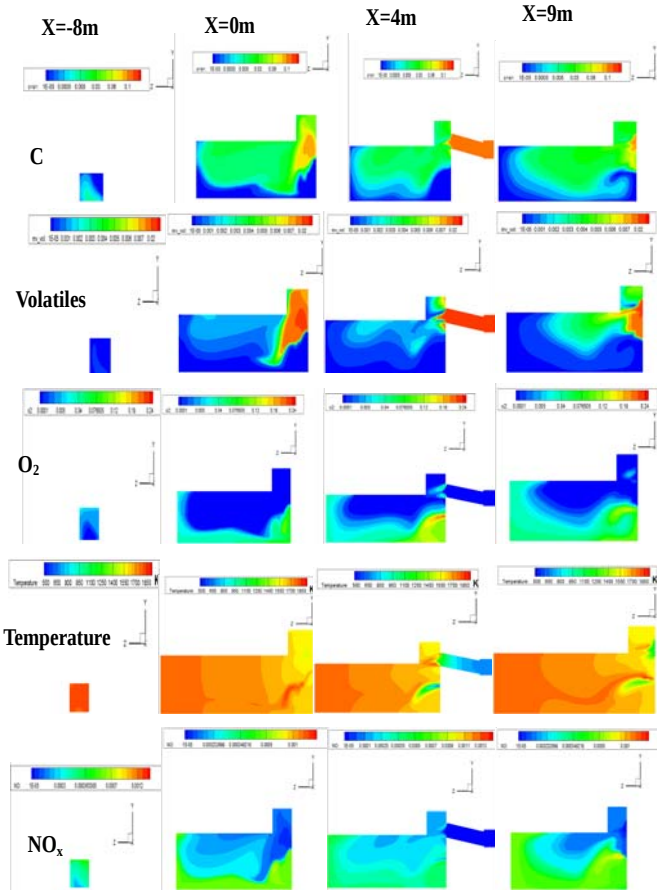

Baseline Case (100% stoichiometric air)

Fig. 10 Species and temperature contour plots on X-direction planes.

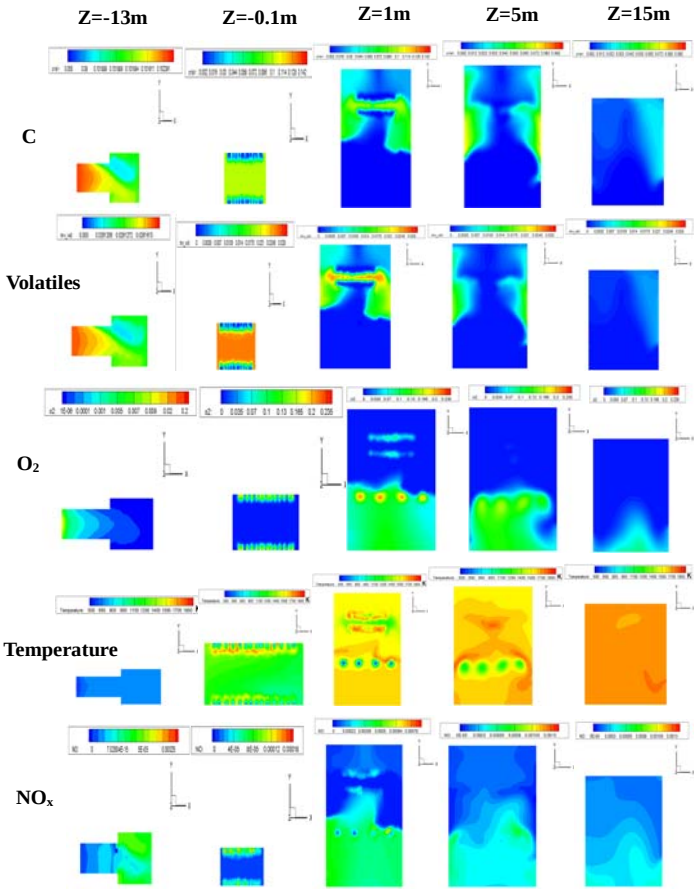

Baseline Case (100% stoichiometric air)

Fig. 11 Species and temperature contour plots on Z-direction planes

Cold air injection from burners can be easily noticed from the blue color. Hot streaks can be clearly identified through X-direction slices in Fig. 5 following the air injection from the burners and the air injection tubes. This can be explained by the following physical process: the fuel (mostly carbon) from the top inlet duct, which is mixed with the air from the air injection tubes, is first partially burned in the high-bay area generating the hot streaks of high-temperature combustion gases; then the remaining fuel, together with the hot combustion gas flow, is directed into the low-bay area to continue to combust with a new supply of the oxygen-rich air flow blown in from the burners. The cold streaks in low-bay area actually show the trace of air flows from the burners. As the combustion intensity decreases along with the air flow moving towards the outlet, mixing effect makes temperature more uniform as shown in temperature contour plots in Figs. 10 and 11 close to the exit region. The function of the high bay wall structure and the distributed second air injection strategy are interesting and will be further examined. From the distributions of velocity field, species concentration and temperature, observations, and analyses are noted below:

- The high-bay wall blocks the inlet flow from directly shooting into the main chamber and slows down the flow in the high bay. Recirculation zones are generated in the high-bay area, which can be seen in Figs. 7, 8 and 9. Thus the high-bay structure slows down the flow velocity, stabilizes the combustion with flow recirculation, and extends the fuel residence time. All of these characteristics help in achieving complete combustion.
- Correspondingly, as shown in Fig. 10, most of the volatiles are combusted in the high bay area, producing high-temperature gases with the highest temperature around 1850 K (2870 ^{o}F).
- For carbon, its combustion also starts and intensifies in the high-bay area. But different from the volatiles combustion, carbon reaction is slower and extends throughout the main chamber. The current length of the pyroscrubber seems necessary to achieve complete carbon combustion.
- The high-bay wall structure forces the flow from the inlet duct to redirect downward to intersect the second air injection from the burners, creating a strong forced mixing of the partially combusted gas from the top and the fresh air from the burners, thus makes combustion take place and generates those hot streaks. This effect of forcing combustion to happen at an earlier stage helps to efficiently utilize the main chamber space and avoid using an otherwise larger main chamber.
- Together with the distributed air injections, the high-bay and low-bay configuration generates a two-stage combustion with 51% stoichiometric air at the first stage in the high-bay area and 49% air at the second stage in the low-bay area, which yields a lower flame temperature than an otherwise one-stage combustion, and thus less NO_x emission. The details of the two-stage combustion will be discussed in the three-stage combustion case (Case 4).
- In the actual operating condition, volatiles are first to be combusted due to their gas phase rather than the carbon particles in solid phase. The combustion in the high-bay area generates high-temperature gases which heat up the carbon particles. This will speed up the combustion process of the carbon particles and reduce the carbon particle sizes and numbers and will allow the smaller carbon particles to remain air borne and prevent more particles from being pulled by gravity (i.e. deposition) to the bottom of the chamber.
- NO_x concentration is generally higher on the bottom of the main chamber than in the upper area, which can be clearly seen from Figs. 10 and 11. It is noticed that NO_x concentration is consistent with O_2 species distribution. Some scattered high concentration spots of NO_x are also found as hot spots or streaks in Figs. 10 and 11. This phenomenon can be explained by the two necessary conditions of NO_x generation: high temperature and sufficient O_2. High NO_x generation rate only happens at places in accordance with these two conditions.
- Flow goes through the outlet duct at a relatively uniform temperature at about 1500 K.

The combustion performance is evaluated and compared at the exit of the pyroscrubber. Together with the inlet conditions, a summary of the exit conditions are shown in Table 3 including the species mass fractions, mass-weighted average temperature, and exergy (useable energy). From Table 3, it is noted that (a) Volatiles are fully combusted inside the main chamber. (b) Small amounts of carbon and oxygen are left in the exit gases. (c) The exit gases mostly consist of N_2 (71%), CO_2 (24%) and water vapor (5%).

Table 3 Simulated results of the baseline case

100% stoichiometric air	main inlet mass (kg/s)	burner-injection (kg/s)	tube-injection (kg/s)	outlet mass (kg/s)	outlet mass fraction
NO_x	0.00	0.00	0.00	0.01	3.24E-04 (321.49 ppm)
Volatiles	0.42	0.00	0.00	0.00	0.00
O_2	0.24	2.66	2.52	0.11	0.00
CO_2	2.16	0.00	0.00	8.73	0.24
H_2O	1.15	0.00	0.00	1.83	0.05
C(s)	1.53	0.00	0.00	0.03	0.00
N_2	9.08	8.82	8.36	26.25	0.71
total	14.58	11.48	10.88	36.95	1.00
Exit Temp	1804K (2788^{o}F)	Exergy	57.17MW		

CFD Validation

The computational simulation is validated by comparing with the actual plant temperature measurement data during operation at three locations: center of the high bay ($\mathbf{T_1}$), center of the main chamber ($\mathbf{T_2}$), and center of the exit duct ($\mathbf{T_3}$). Also, the NO_x emission result from the simulation is compared with the plant operating data. The results are summarized in Table 4.

Table 4 Comparison between measured data and baseline simulation results

	T_1 (K)	T_2 (K)	T_3 (K)	NO_x (kg/hr)
Measured Data	1616	1616	1533	35 - 45
Simulation	1804	1770	1641	43.2
Difference	11.63%	9.53%	7.05%	within range

The comparison in Table 4 shows that the simulation results seem to overpredict temperature consistently around ten percent at all three measurement locations. Considering that the simulation assumes adiabatic wall condition, it is reasonable to interpret that the relatively lower measured temperature is partially attributed to heat losses through the walls in the real environment. The plant operators also report that they often provide 5-10% more air than stoichiometric value to ensure more complete combustion in most part of the pyroscrubber and hence to reduce carbon monoxide. The excessive air, therefore, also contributes to reduced temperature. NO_x prediction from the simulation (43.2 kg/hr) falls within the range of measured data (35 - 45 kg/hr) and is a bit on the higher end of the measured range due to higher simulated temperature. Based on these comparisons, the simulation model set up in this study is considered trustful and acceptable.

Case 2: 80% Stoichiometric Air Combustion

To find out the effect of less than stoichiometric air injection on the pyroscrubber's combustion performance, 80% stoichiometric air combustion case is simulated with eddy-dissipation model. Temperature and species distribution, flow velocity field, NO_x emission information, and exergy of combusted gases will be evaluated, and comparisons are to be made with the baseline case.

Temperature contours of different planes in X, Y and Z directions are shown in Fig. 12. It can be immediately noticed that the overall temperature is lower than the baseline case. This is expected due to the incompleteness of the fuel combustion and correspondingly less energy being released inside the main chamber. Hot streaks can still be seen but with decreased temperature from the baseline case. The temperature distribution pattern is very similar to the baseline case.

The inlet conditions and the simulated results of Case 2 with mass weighted species and temperature at the exit are shown in Table 5. The results show that most of the volatiles (88%) are combusted in the main chamber. All oxygen is consumed inside the pyroscrubber, which is consistent with the 80% stoichiometric air injection rate (fuel rich). 21% of the carbon is not burned. The mass-averaged outlet flow temperature is about 100K lower than the baseline case (100% stoichiometric air). NO_x emission is greatly reduced to 8.3% of the baseline case. This can be explained as a result of two main reasons: (a) Lower combustion temperature: Less fuel is combusted resulting in lower combustion temperature, which is a favorable factor to reduce NO_x production. (b) Less oxygen: Oxygen is mostly consumed by the fuel (volatiles and carbon) and results in a reduction of NO_x generation. Total exergy is reduced to 83% of the baseline case.

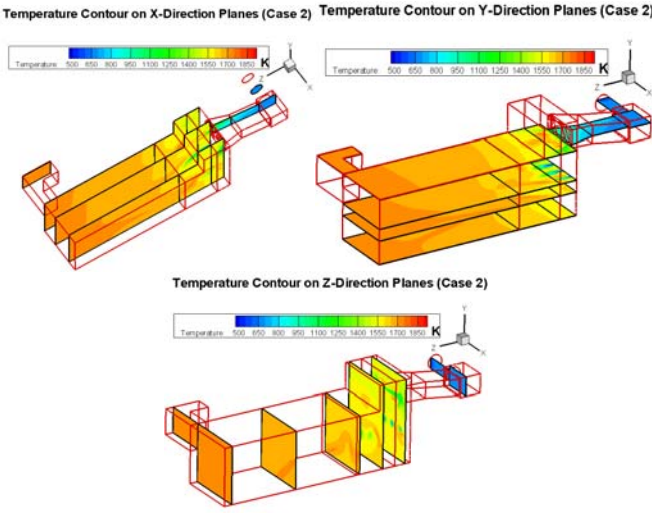

80% stoichiometric air combustion

Fig. 12 Temperature contour inside the pyroscrubber for different planes for 80% stoichiometric air combustion

Summary of Case 2:

- In term of NO_x emission control, the pyroscrubber performance is very good at 80% stoichiometric air injection condition with an order of magnitude reduction of NO_x.
- One major drawback of sub-stoichiometric combustion is the losses of fuel and exergy, which will affect electricity production of the steam power plant.
- 80% air running condition yields lower exit gas temperature, which will result in lower boiler and steam turbine efficiency. Thus less electricity is to be produced.
- CO emission is a concern with the 80% stoichiometric air combustion condition due to reduced combustion temperature and the fuel-rich combustion pattern. No simulation of CO production is performed in gas combustion model in this study, but it will be discussed in the heterogeneous combustion model in a future paper. .
- Overall, incomplete combustion at sub-stoichiometric air combustion case is not a favorable running condition for the pyroscrubber. It is necessary to generate a complete combustion condition to utilize all the energy from the fuel.

Table 5 Simulated results of 80% stoichiometric air combustion case

80% stoichiometric air	main inlet mass flow rate (kg/s)	burner-injection (kg/s)	tube- injection (kg/s)	outlet mass flow rate (kg/s)	outlet mass fraction
NO_x	0.00	0.00	0.00	0.001	3.02E-05 (29.37 ppm)
Volatiles	0.42	0.00	0.00	0.05	0.00
O_2	0.24	2.13	2.02	0.00	0.00
CO_2	2.16	0.00	0.00	7.53	0.23
H_2O	1.15	0.00	0.00	1.76	0.05
C(s)	1.53	0.00	0.00	0.32	0.01
N_2	9.08	7.06	6.69	22.81	0.71
total	14.58	9.19	8.71	32.47	1.00
Exit Temp	1726K (2647 °F	Exergy	47.32MW		

Case 3: 150% Stoichiometric Air Combustion

As an 80% stoichiometric air combustion case is studied as the lower limit of the incomplete combustion running condition of the pyroscrubber, 150% air combustion case is studied as the higher limit of excess air combustion condition. From the discussion of 80% air combustion (Case 2), it is concluded that all fuel must be combusted to fully utilize the fuel's energy and in the meantime the combusted temperature needs to be reduced to decrease NO_x formation. With the 150% stoichiometric air, this goal is expected to be achieved, although it is understood that the energy density could be reduced.

Temperature contour plots for different planes are shown in Fig. 13, and the velocity plots are shown in Figs. 14, 15 and 16. The results indicate:

• The overall combustion temperature is lower than both the baseline case (Case 1) and the 80% stoichiometric combustion case (Case 2).

• Hot streaks can still be identified; but are much weaker, i.e. with smaller volumes and lower temperatures, than in Cases 1 and 2.

• Temperature distribution in the main chamber is more uniform than both of Cases 1 and 2. This can be explained by the following reasons:

(a) The combustion is less intensive due to diluting effect of the excess air. With more air, the species concentration of fuels is reduced, and thus generates slower reaction rates.

(b) Stronger mixing effect can be found from Figs. 14, 15 and 16. Larger amounts of air injected from tubes and burner slot produces higher air speed and stronger mixing effect than in Cases 1 and 2.

• Two visible recirculation zones can be seen from Fig. 14. One is at the high-bay area, where the flow from the inlet duct impinging to the high-bay walls generates the recirculation zone. The other one is close to the burner slots where burner air injection intersects the gas flow bending down from the top. The strengths of both recirculations are stronger than in Cases 1 and 2.

• From Fig. 15, at Y=0.1m close to the bottom of the main chamber, flow is found to be separated into two streams in the 2-D plot, indicating the existence of a stagnation region. This is the result of the flow bending down from the top impinging to the bottom floor. Comparing with the velocity profiles of the baseline case and 80% air combustion case, it is noticed that the location of flow separation has moved downstream due to stronger flow injection of the 150% air combustion case.

• At Z=15m, the velocity profile is very different from both Cases 1 and 2. Recirculation can still be clearly identified at this location for the 150% air case, suggesting a much stronger mixing compared with Cases 1 and 2.

• At Z=35m, recirculation zones disappear and the flow becomes more uniform, similar to the baseline case and 80% air case.

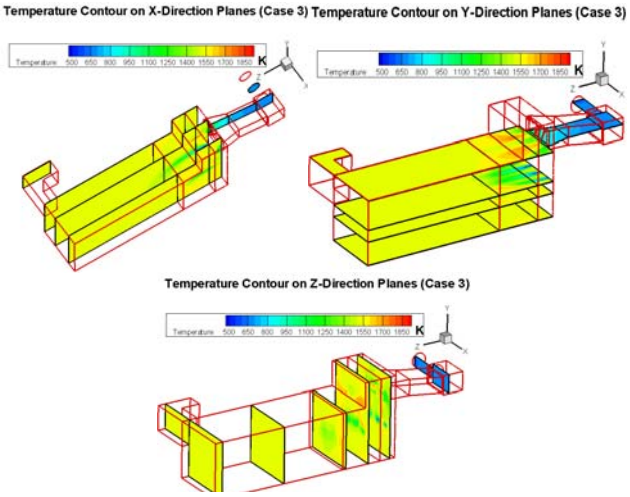

150% stoichiometric air combustion

Fig. 13 Temperature contour inside the pyroscrubber for Case 3 with 150% stoichiometric air combustion.

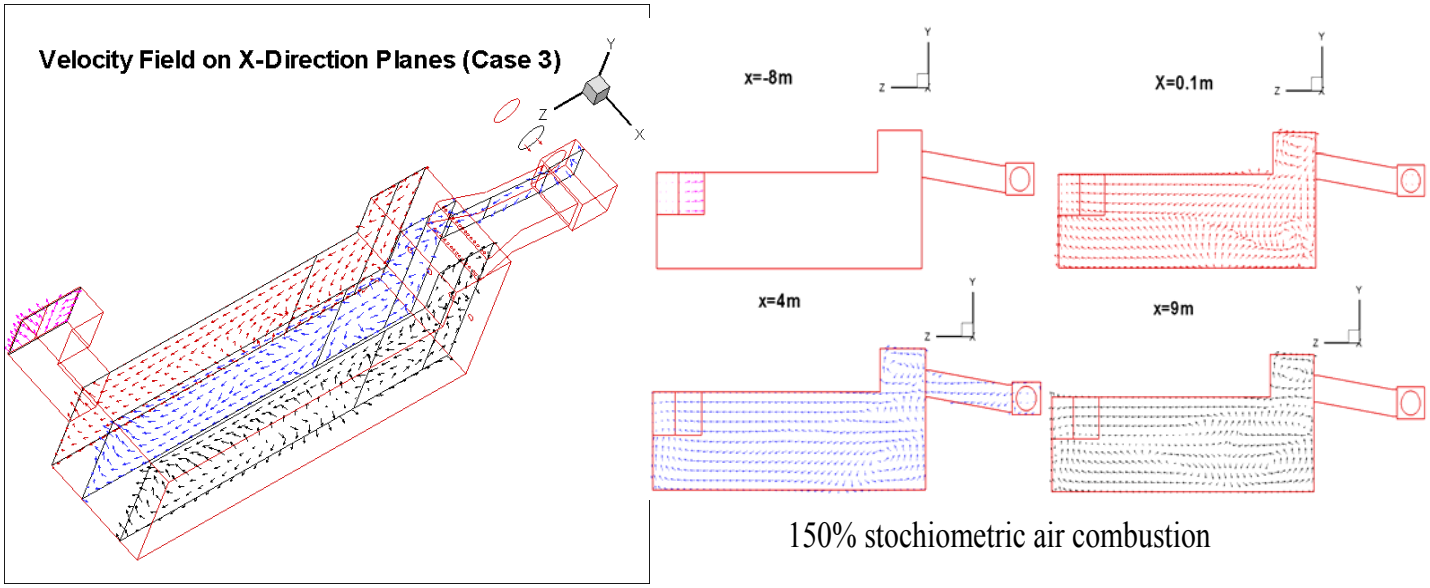

Fig.14 Velocity fields on X-direction planes for 150% stoichiometric air combustion

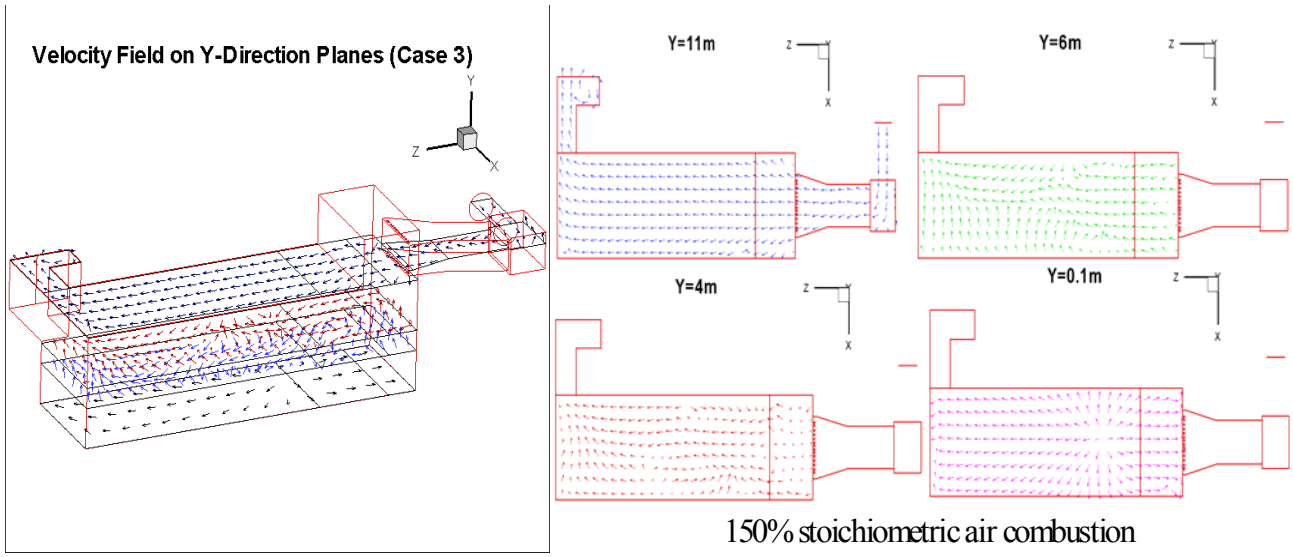

Fig. 15 Velocity fields on Y-direction planes for 150% stoichiometric air combustion (Case 3)

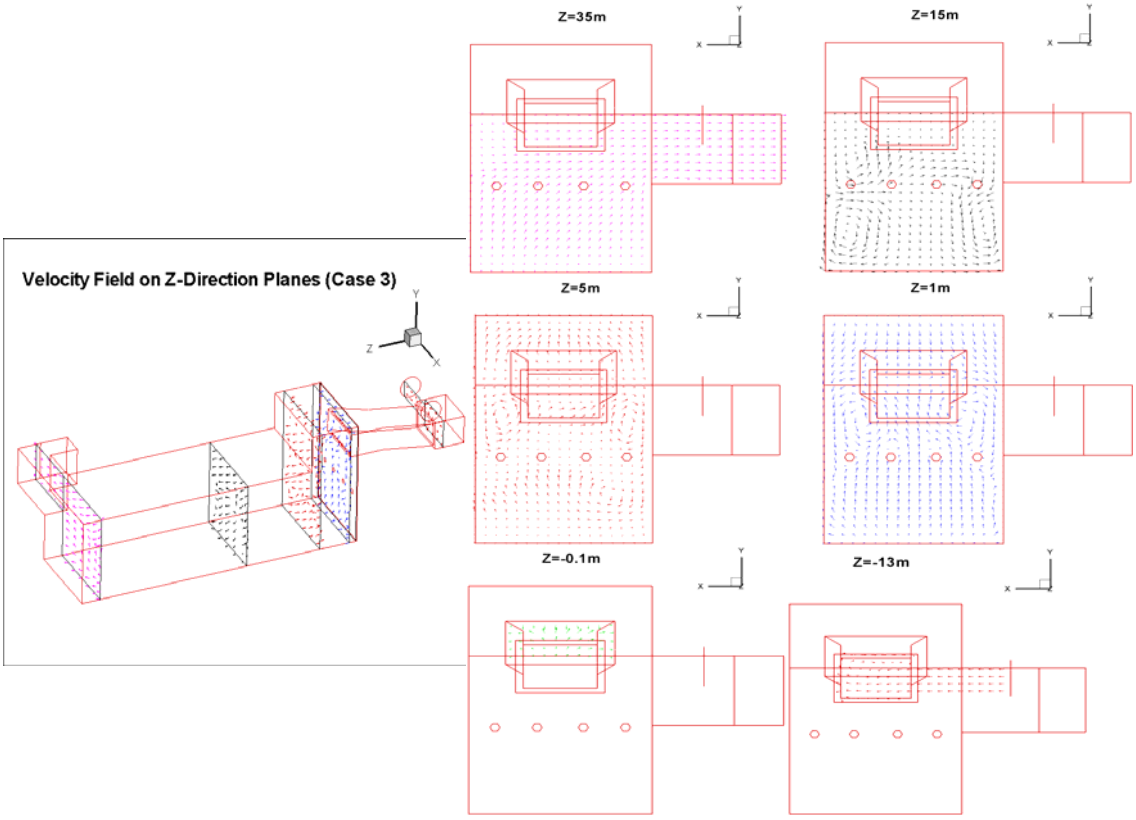

150% stoichiometric air combustion

Fig. 16 Velocity fields on Z-direction planes for 150% stoichiometric air combustion (Case 3)

The inlet condition and the simulated results at exit of Case 3 are tabulated in Table 6. The results show that:

• All the volatiles and carbon are burned inside the pyroscrubber, which is expected for combustion with a large amount of excess air.

• Much lower outflow temperature is found (281K and 203K lower than 100% and 80% air combustion respectively), indicating that cold excess air cools down the combustion gas.

Table 6 Simulated results of 150% stoichiometric air combustion case (Case 3)

150% stoichiometric air	main inlet mass flow rate (kg/s)	burner-injection (kg/s)	tube-injection (kg/s)	outlet mass flow rate(kg/s)	outlet mass fraction
NO_x	0.00	0.00	0.00	4.00E-04	7.56E-06 (7.45 ppm)
Volatiles	0.42	0.00	0.00	0.00	0.00
O_2	0.24	4.00	3.79	2.64	0.05
CO_2	2.16	0.00	0.00	8.82	0.18
H_2O	1.15	0.00	0.00	1.83	0.04
C(s)	1.53	0.00	0.00	0.00	0.00
N_2	9.08	13.22	12.54	34.84	0.73
total	14.58	17.22	16.33	48.13	1.00
Exit Temp	1523K (2282 °F)	Exergy	56.17 MW		

• NO_x emission is significantly reduced to 2.3% of the baseline case and 25% of Case 2 in term of NO_x mass flow rate (kg/s). The lower emission value based on mass fraction could be misleading because the mass fraction is diluted by the excessive air mass. So, a more meaningful method is to compare the mass flow rates of the emissions (kg/s), which shows the mass flow rate of NO_x of the 150% case is 3.3% of Case 1 and 40% of Case 2 values, respectively.

• The result shows that even though there is more oxygen in 150% air combustion case, the reduced combustion temperature seems to effectively cut down the NO_x emission.

• The total exergy is about the same as the baseline case due to the complete combustion.

Summary Case 3:

• In terms of NO_x emission control, the pyroscrubber performance is best with 150% stoichiometric air. It gives the lowest NO_x emission in either mass fraction or mass flow rate.

• The major draw-back of 150% air running condition is the much lower output gas temperature. When the outflow gas is used in boiler, it will decrease the overall efficiency of the power generation system.

• Overall, Case 3 undergoes a complete combustion that harvests full energy from the fuel. Excess air cools down the combusted gas temperature and significantly cuts down NO_x emission. Balance between these two effects need to be made to obtain the optimum pyroscrubber performance.

Case 4: Three Stage Combustion (41%, 39% and 20%)

Based on the results and discussions from the baseline case, two limiting cases of incomplete combustion (80% stoichiometric air) and excess-air combustion (150% stoichiometric air), a new burning strategy by distributing air injection into three stages is studied. In addition to the existing two-stage combustion of Case 2 in the high-bay and low-bay regions, an additional 20% stoichiometric air is injected through the side doors in the outlet duct walls to burn off all the fuel. The theory of employing the three-stage combustion is to cut down the NO_x emission by distributing the third air injection much further downstream to reduce the flame temperature in the early stage of combustion. The reason for choosing the third stage in the outlet duct is because the main chamber of the pyroscrubber is too spacious to achieve uniform combustion with localized air injection, whereas it is thought that it will be easier to achieve uniform combustion in the outlet duct since the flow converges into much smaller space in the outlet duct. (The latter reasoning is later found not holding as wished.) Meanwhile the exit temperature will not be compromised such as in Cases 2 or 3.

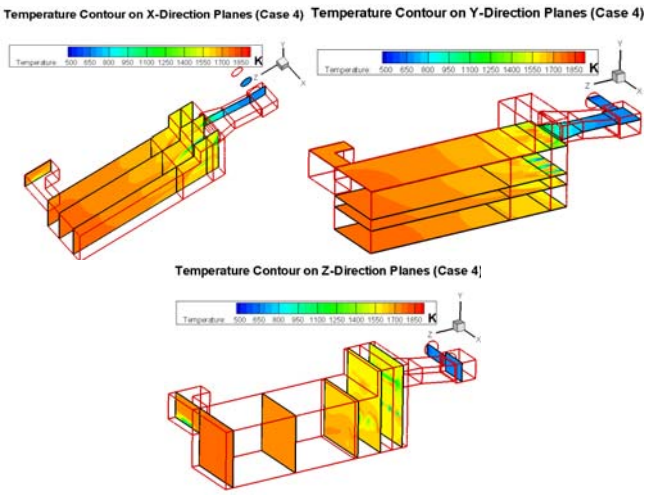

Three stage combustion (41%, 39% and 20%)

Fig. 17 Case 4 temperature contour inside the pyroscrubber with three-stage combustion (41%, 39% and 20%)

Figures 17 and 18 show the temperature contour plots and velocity field for the three-stage combustion case (Case 4). The inlet conditions and the results at exit are shown in Table 7. The results show that as expected, the temperature profiles are very similar to 80% case in regions of inlet duct and the main chamber. The difference occurs in the region close to the third stage air injection in the outlet duct where the temperature distribution is relatively non-uniform

The fuels are not completely combusted as there is carbon left in the outlet species as shown in Table 7. Five percent of the volatiles and 12% of the carbon (based on the inlet mass flow rate) are left unburned in the outflow gas.

Outflow temperature is 100K lower than the baseline case and close to 80% case, but is higher (200k) than the 150% case. This can be explained as that despite the fact more fuel is burned in the three-stage burning case and more energy is released into the gas than Case 2 of 80% air, the combustion is not complete in the third stage, perhaps due to the short residence time inside the outlet duct. Furthermore, introduction of cold air at this late stage cools down the gas. These two factors counteract each other and thus the temperature is about the same as 80% air case (Case 2).

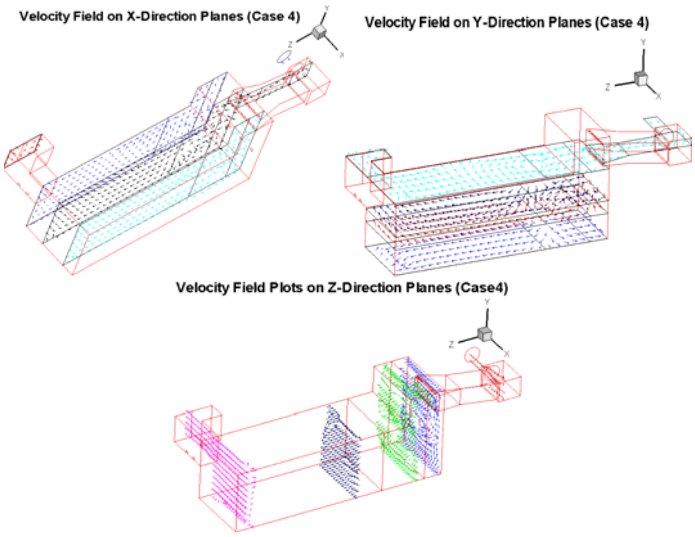

Three stage combustion (41%, 39% and 20%)

Fig. 18 Velocity fields for 3-stage combustion in Case 5.

NO_x emission is cut down to 15.8% of the baseline case, but is 190% higher than the 80% air case (Case 2) and 475% higher than the 150% air case (Case 3). The exit exergy is slightly below the baseline case (91%) and 150% air case (93%), but is higher than 80% air case (110%).

Table 7 Simulated results of three-stage burning case (Case 4)

three-stage combustion (41%, 39% and 20%)	main inlet mass flow rate(kg/s)	burner-injection (kg/s)	tube-injection (kg/s)	near-exit air injection	outlet mass flow rate(kg/s)	outlet mass fraction
NO_x	0.00	0.00	0.00	0.00	1.90E-03	5.24E-04 (51.36 ppm)
Volatiles	0.42	0.00	0.00	0.00	0.02	0.0005
O_2	0.24	2.13	2.02	1.04	0.72	0.02
CO_2	2.16	0.00	0.00	0.00	8.01	0.22
H_2O	1.15	0.00	0.00	0.00	1.79	0.05
C(s)	1.53	0.00	0.00	0.00	0.19	0.01
N_2	9.08	7.06	6.69	3.44	26.21	0.70
total	14.58	9.19	8.71	4.47	36.94	1.00
Exit Temp	1702K (2604 ^oF)	Exergy	52.20 MW			

Summary of Case 4:

- For NO_x emission control, the three-stage burning strategy can successfully cut down the emission in comparison with the baseline case.
- Although the NOx emission of the three-stage burning case is higher than 80% case and 150% case, Case 4 doesn't have the drawbacks of either compromised exergy in the 80% air case or reduced exit temperature in the 150% air case.
- It should be noted that the current 41%, 39% and 20% composition of air injection load is not the optimized air distribution, as can be seen from Table 7 that carbon species still exists in the outflow, meaning the fuel is not completely burned under the simulated three-stage air distribution. Further studies will be needed to optimize the multi-stage combustion strategy.
- The existing doors on the side walls of the outlet duct are used for convenience in the third stage air injection. Since the locations of the doors are close to the exit and the space inside the outlet duct is relatively small, two issues are encountered (a) The duct is not long enough to provide sufficient residence time to achieve complete combustion before the flow exits; (b) Due to the short residence time, the combustion takes place locally without sufficient time to propagate through the entire duct and hence, hot spots form and NO_x emission increases. Further studies are needed to improve the selection of third-stage air injection and the air injection pattern.

CONCLUSIONS

Comparisons of Cases 1-4 (100%, 80%, 150% and Three-Stage Cases) are shown in Table 8:

Table 8 Summary of four simulated results

cases	total energy output(MW)	estimated power generation (MW)#	mass flow rate (kg/s)	temperature (K)	NOx emission (kg/s)	NOx emission (ppm)
100%	57.17	17.01	36.94	1804	0.0120	321.49
80%	47.32	14.08	32.47	1726	0.0010	29.37
150%	56.17	16.71	48.13	1523	0.0004	7.45
3-stage	52.20	15.53	36.94	1702	0.0019	51.36

The estimated power generation is based on 85% of boiler efficiency and 35% of steam turbine efficiency. For 150% case, the estimated power generation shown is over-estimated because its exit temperature is 300K lower than other cases and the boiler efficiency will be lower than 85%.

The comparison show:

- The three-stage burning strategy can effectively reduce NO_x emission without compromising total energy output.
- Excess air can help to reduce NO_x emission and increase total energy output, but yields lower output gas temperature which will reduce boiler efficiency. A well balanced amount of excess air is favorable.
- Incomplete combustion with sub-stoichiometric air cuts NO_x emission, but leads to less total energy output, lowers gas temperature and increased CO emission.

ACKNOWLEDGEMENTS

This study was supported by Rain CII Carbon, LLC. Part of the funding was provided by the Louisiana Board of Regents' Industrial Ties Research Subprogram.

REFERENCES

[1] Baulch, D. L., Drysdall, D. D. and Lloyd, L. C., "Evaluated Kinetic Data for High Temperature Reactions," Butterworth, volume 1,2,3. 1973.

[2] Blauvens, J., Smets, B. and Peters. J., 16th Symp. (Int'l.) on Combustion. The Combustion Institute, 1977.

[3] Byrne, Henry James, United States Patent 4,012,202, 1977.

[4] CII Carbon, LLC., "CII Rotary Coke Calciner Modeling-1D Coke Calcination," Internal report, Vol. 2. 2004

[5] Eggels, R.L.G.M., "Modeling of NO_X Formation of a Premixed DLE Gas Turbine Combustor," Proceedings of ASME TURBO EXPO, June 2001.

[6] Fluent 6.3 User's Guide, September 2006, Fluent Inc.

[7] Hanson, R. K. and Salimian, S., "Survey of Rate constants in H/N/O Systems," Combustion Chemistry, page 361, 1984.

[8] Magnussen, B. F. and Hjertager, B. H. "On mathematical models of turbulent combustion with special emphasis on soot formation and combustion," 16th Symp (Int'l) on Combustion, The Combustion Institute, 1976.

[9] Zhao, L. and Wang, T.," Simulation of Combustion and Thermal-flow Inside a Pyroscrubber," ECCC Report 2008-02, Energy Conversion and Conservation Center, University of New Orleans, August 2008.

[10] Zhang, Z. and Wang, T.," Thermal-Flow and Combustion Simulation in a Rotational Calcining Kiln," ECCC Report 2007-02, Energy Conversion and Conservation Center, University of New Orleans, submitted to CII Carbon, LLC. 2007.

[11] Faeth, G. M., "Mixing, Transport, and Combustion in Sprays," Prog. Energy Combust. Sci., Vol. 13, pp. 291-345, 1987.